Dependence of IR-Bright AGN Activity on Halo Mass and Redshift in the SPT Cluster Surveys

Benjamin Floyd [1] Mark Brodwin [1] Rebecca E. A. Canning [2] The SPT Collaboration

[1]University of Missouri–Kansas City [2]University of Portsmouth

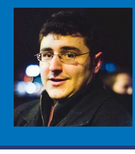

Motivation

We know that environment plays a role in galaxy evolution (e.g., Dressler, 1980, 1984), but how exactly? What are the predominant environmental-dependent mechanisms that are behind the rapid mass assembly (Mancone et al., 2010), enhanced star formation (Brodwin et al., 2013) and increased AGN activity (Martini et al., 2013) that has been observed in galaxy clusters at high-redshift ($z \gtrsim 1.4$). Independently both Brodwin et al. (2013) and Ehlert et al. (2015) arrived at similar conclusions that galaxy–galaxy merging within the clusters may be the mechanisms driving galaxy evolution in galaxy clusters early in their history. In sufficiently gas-rich galaxy–galaxy merging, the gas will be dynamically disrupted triggering both enhanced star-formation activity and allows for gas to funnel into the galactic nucleus and accrete onto the central supermassive black hole creating an AGN.

Similar to Ehlert et al. (2015), we aim to model the AGN incidence in galaxy clusters as tracers of galaxy evolution of the cluster members.

SPT Cluster Sample

Our cluster sample derives from two galaxy cluster surveys carried out by the 10-meter South Pole Telescope (SPT; Carlstrom et al., 2011) the 2500 deg^2 SPT-SZ survey (Bleem et al., 2015) and the deep, 100 deg^2 SPTpol 100d survey (Huang et al., 2020). Combined we have a cluster sample of over 300 clusters with a median redshift of $z \sim 0.69$ and median cluster mass of $M_{500} \sim 3.73 \times 10^{14} M_\odot$.

By using the SPT cluster surveys we are able to span a wide range of redshifts (see Fig 1.) and as the SPT detects clusters using the Sunyaev–Zel'dovich Effect (SZE) we have an effectively uniform-selected mass sample.

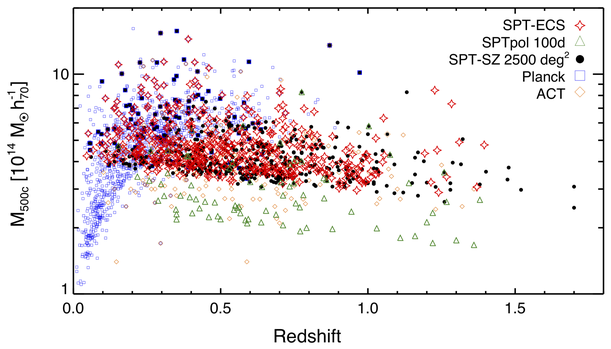

Figure 1. Mass and redshift distribution of the SPT cluster surveys.

IR-Bright AGN Selection

Our AGN are selected using *Spitzer*/IRAC imaging in 3.6 μm and 4.5 μm wavelengths. We find a color selection of $[3.6\ \mu\text{m}] - [4.5\ \mu\text{m}] \geq 0.7$ to be optimal in selecting AGN that would have been otherwise selected by a IRAC color-color selection (e.g., Stern et al., 2005) as shown in Figure 2. Furthermore, to account for Eddington bias in the form of photometric uncertainty we employ a fuzzy membership selection to our data in order to create the final sample as seen in Figure 3. Using our selection criteria, we select ~ 2200 AGN candidates.

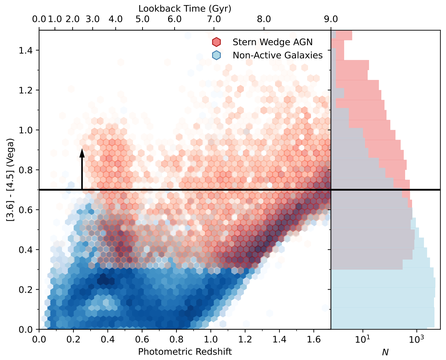

Figure 2. IRAC colors of all objects in the Spitzer Deep Wide-Field Survey (SDWFS; Ashby, Stern, et al., 2009) detected in 4.5 μm with SNR ≥ 5. Red points are objects that satisfy the AGN selection criterion as described in Stern et al. (2005). Blue hexbins are SDWFS objects that do not fall within the Stern wedge criterion. Our IRAC color selection is shown as the solid black line.

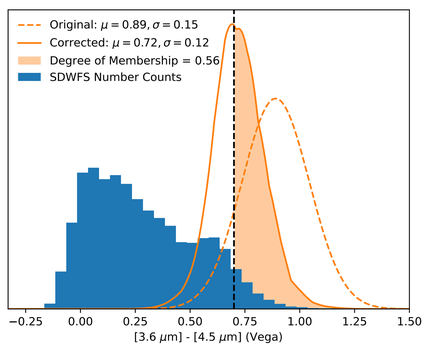

Figure 3. Example of applying our Eddington bias correction and computing degrees of membership into our AGN sample. The original color and color error of the object is assumed to form a Normal distribution as given by the dashed curve which is then convolved with the deeper SDWFS number count distribution to account for Eddington bias. The object's degree of membership into our sample is given by the integral of the corrected color (solid curve) above our cut off.

Preliminary Trends

Preliminary analysis on the our data sample and has found some initial interesting trends such as indications of an inverse trend of AGN richness with cluster mass at a fixed redshift as can be seen in Figure 4. This agrees well with the expectations from Brodwin et al. (2013) and the measurements from Ehlert et al. (2015).

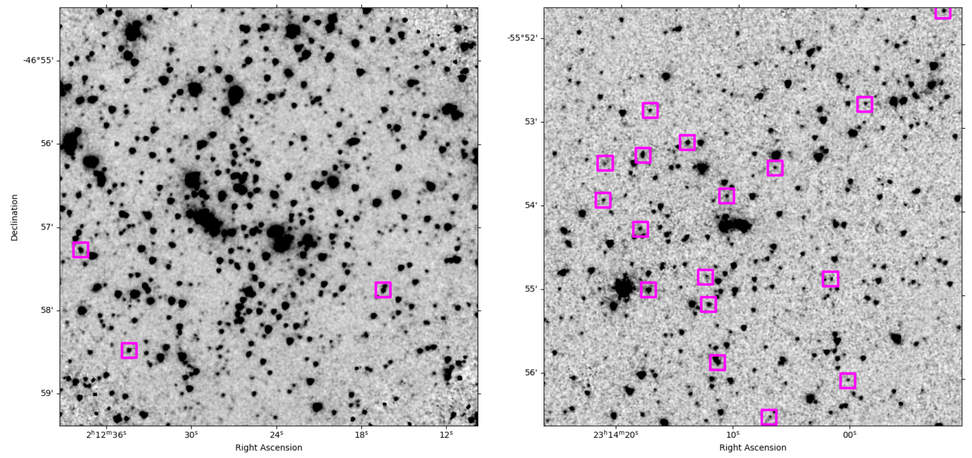

Figure 4. IRAC 3.6 μm images of SPT cluster around the median redshift of our sample. IR-bright AGN are marked by magenta boxes. (left) SPT-CL J0212-4657 $M_{500} = 6.06 \times 10^{14} M_\odot, z = 0.65$; (right) SPT-CL J2314-5554 $M_{500} = 2.18 \times 10^{14} M_\odot, z = 0.71$.

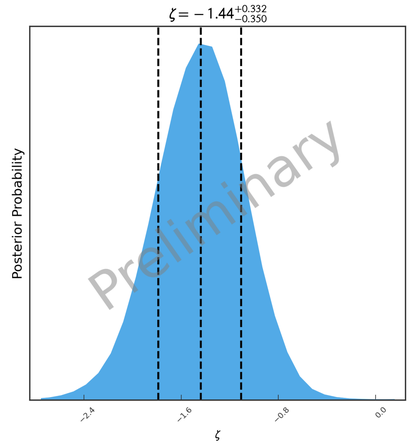

Figure 5. Preliminary posterior probability of the mass parameter for our SPTcl-IRAGN sample.

Bayesian Modeling

We model AGN incidence along the line-of-sight to a cluster as power laws in redshift and cluster mass and use a beta model to describe the projected cluster-centric radial distribution. The background contamination is modeled as a constant additive quantity.

Model

$$N(z, M_{500}, r) = \theta(1+z)^\eta \left(\frac{M_{500}}{10^{15} M_\odot}\right)^\zeta \left[1 + \left(\frac{r}{r_c}\right)^2\right]^{-1.5\beta+0.5} + C$$

Likelihood

$$\ln \mathcal{L}(\theta, \eta, \zeta, \beta, r_c, C) \propto \sum_j^{N_{\text{cl}}} \left[\sum_i^{N_{\text{AGN}}} \ln\left(N_{ji} r_i m_{\text{AGN},i}\right) - w_{\text{comp}} \int_0^R N_j 2\pi r \, \mathrm{d}r\right]$$

To validate our probabilistic model and establish expected variances on model parameters we created mock data sets that mimic our real data using model parameter sets chosen to test the expected parameter ranges.

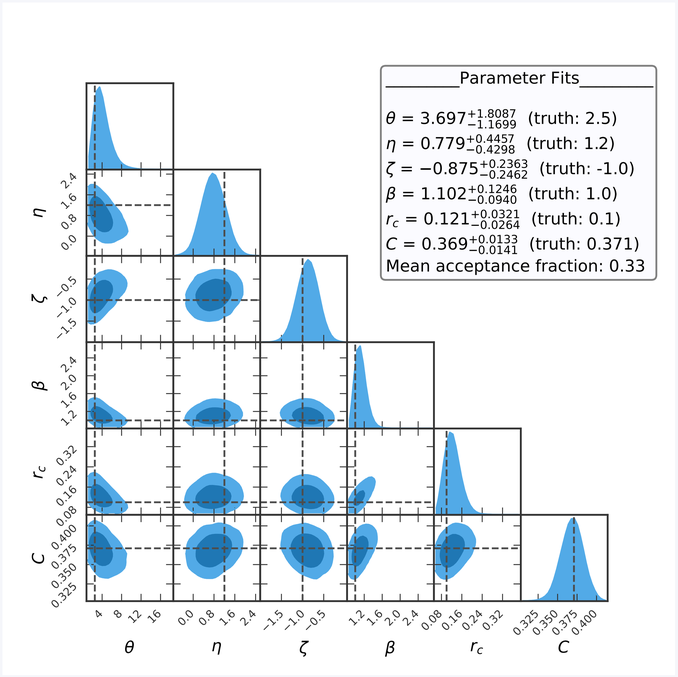

Figure 6. Model parameter fits from realistic mock catalog with input parameters indicated by dashed lines.

Mock Catalog

We generate our mock catalogs using an Inhomogeneous spatial Poisson point process that uses our model to generate both cluster and background sources. Model parameters are chosen from physically motivated values and calibrated to mimic the number counts in our real data set. Cluster information (e.g., redshifts, M_{500}, cluster centers) are sourced randomly from the SPT cluster catalogs while object information (e.g., photometric completeness correction, fuzzy degree of membership) are sourced randomly from our SPTcl-IRAGN data sample.

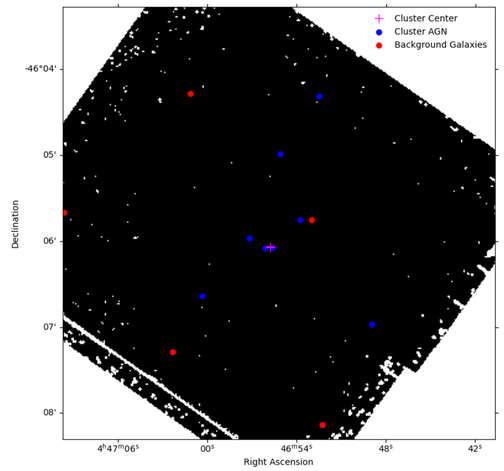

Figure 7. Example of a mock cluster with a background mask showing the area of the simulated image above our coverage threshold.

Ongoing Work

Due to issues with our redshift trend in earlier analyses, we are now working on including a luminosity function into our model to account for the luminosity evolution of AGN as a function of redshift. To accomplish this, we have elected to implement the IR-bright AGN luminosity function with luminosity and density evolution from Assef et al. (2011).

$$\begin{cases} \Phi(M_J, z) = 0.4 \ln(10) 10^{0.4(M_{*,J}(z) - M_J)} \Phi_*(z) \left[10^{-0.4\alpha_1(M_{*,J}(z) - M_J)} + 10^{-0.4\alpha_2(M_{*,J}(z) - M_J)}\right]^{-1} \\ M_{*,J}(z) = \sum_{i=1}^{4} M_{*,J}(z_i) \prod_{k=1, k\neq i}^{4} \frac{z - z_k}{z_i - z_k} \\ \log[\Phi_*(z)] = \sum_{i=1}^{5} \log[\Phi_*(z_i)] \prod_{k=1, k\neq i}^{5} \frac{z - z_k}{z_i - z_k} \end{cases}$$

We then update our model accordingly,

$$N(z, M_{500}, r) = \theta D_A(z)^2 r_{500} \Phi(M_J, z)(1+z)^\eta \left(\frac{M_{500}}{10^{15} M_\odot}\right)^\zeta \left[1 + \left(\frac{r}{r_c}\right)^2\right]^{-1.5\beta+0.5} + C$$

We are currently working with updated mock catalogs to validate our modifications to our model and likelihood. Once validations are complete we will begin refitting our data sample using the updated model.

References

M. L. N. Ashby, S. A. Stanford, et al., ApJS **209**, 22, 22 (2013). M. L. N. Ashby, D. Stern, et al., ApJ **701**, 428 (2009). R. J. Assef et al., APJ **728**, 56, 56 (2011). L. E. Bleem et al., ApJS **216**, 27, 27 (2015). M. Brodwin et al., ApJ **779**, 138, 138 (2013). J. E. Carlstrom et al., PASP **123**, 568 (2011). A. Dressler, ApJ **236**, 351 (1980). A. Dressler, ARA&A **22**, 185 (1984). S. Ehlert et al., MNRAS **446**, 2709 (2015). N. Huang et al., AJ **159**, 110, 110 (2020). C. L. Mancone et al., ApJ **720**, 284 (2010). P. Martini et al., ApJ **768**, 1, 1 (2013). D. Stern et al., ApJ **631**, 163 (2005).